

Multiscale Models of Electrochemically-Promoted Large Catalytic Surfaces

Ioannis S. Fragkopoulos and Constantin Theodoropoulos

School of Chemical Engineering and Analytical Science, University of Manchester, Sackville Street, Manchester, U.K.

Keywords: Electrochemical Promotion of Catalysis, CFD-KMC Coupling, Gap-tooth Method, Lattice-lattice Interactions, CO Oxidation on Pt/YSZ.

Abstract: In the current work a multiscale framework for electrochemically promoted catalytic systems is formulated. It integrates a macroscopic model based on commercial CFD software, which simulates the charge transport in the system, and an in-house developed efficient implementation of the kinetic Monte Carlo method for the simulation of reaction-diffusion micro-processes taking place on the catalyst. The “large” catalytic surface is split into a number of smaller “representative” lattices whose total area is only a fraction of the actual catalytic area. Efficient coarse-graining methodologies based on equation free methods (Gear et al., 2002) are employed to simulate the interactions between these lattices including lateral (lattice-to-lattice) transport through diffusion. Hence, the computationally intensive microscopic simulations are handled with efficiency.

1 INTRODUCTION

The aim of this work is the construction of an accurate multiscale framework for electrochemically promoted large catalytic systems. Electrochemical Promotion of Catalysis (EPOC), also termed as Non-Faradaic Electrochemical Modification of Catalytic Activity (NEMCA), is the enhancement of catalytic activity due to an electrochemically controlled migration of “backspillover” species, i.e. $[O^{\delta-} - \delta+]$, from the solid electrolyte to the catalytically active, gas exposed, electrode surface, when potential is applied between the two electrodes of the solid electrolyte cell. Oxygen anions are excorporated from the Triple Phase Boundaries (TPBs), i.e. places where gas phase, metal and electrolyte meet (Fig.1), forming BackSpillover Species (BSS). The BSS spill over the catalytic surface forming an effective double layer, which affects the binding strength of the chemisorbed reactants. The EPOC phenomenon was first observed by Stoukides and Vayenas (1981) and has since been of increasing interest in the field of modern electrochemistry (Poulidi et al., 2011). It was also found that EPOC can lead to up a 600% increase in the surface reaction rate and sometimes is maintained under current interruption (Yentekakis et al., 1994). Few modelling studies have addressed

this phenomenon. Most relevant works focus on the kinetics of the catalytic surface.

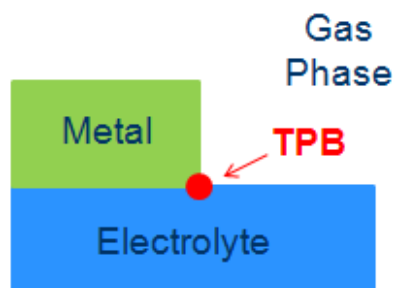


Figure 1: The Triple Phase Boundary.

In previous work (Fragkopoulos et al., 2012) we have proposed, for the first time, an accurate multiscale model of electrochemical promotion, taking explicitly into account all interactions between different length scales. In this work we extend our multiscale model to handle larger catalytic surfaces employing intelligent interpolation techniques (Gear et al., 2003); (Armaou et al., 2005). Thus, the computationally expensive (or even intractable) large microscopic simulations are performed with efficiency.

2 PHYSICS OVERVIEW

2.1 The Computational Domain

The 3D computational domain of the solid oxide single pellet we consider here is depicted in Fig. 2. It consists of an electrolyte (YSZ), an adjacent catalytic film (Pt) as working electrode and an (also adjacent) counter electrode (Au) which is assumed to be inert. Both Pt and Au electrodes are considered as 2D surfaces with infinitesimal heights. The physical dimensions of the system are illustrated in Fig. 2 where $L_{el}=500\text{nm}$, $W_{el}=100\text{nm}$, $H_{el}=5\mu\text{m}$, $a=34\text{nm}$ and $b=152\text{nm}$. CO oxidation on Pt/YSZ is the reaction framework of choice.

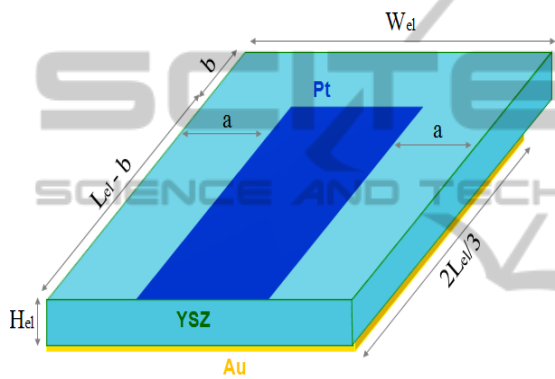


Figure 2: The 3-D Computational Domain.

2.2 The Electrochemical Process

When potential is applied between the anodic and cathodic electrodes of the pellet, charge is transferred throughout, due to electrochemical reactions (presented in Table 1) taking place at the TPBs of anode and cathode.

Table 1: The scheme of electrochemical reactions.

Cathodic TPB:	$3 \times \left[\frac{1}{2} O_{2(g)} + 2e^- \rightarrow O_{YSZ}^{2-} \right]$	(1)
	$O_{YSZ}^{2-} + CO_{(g)} \rightarrow CO_{2(g)} + 2e^-$	(2)
Anodic TPB:	$O_{YSZ}^{2-} \rightarrow \frac{1}{2} O_{2(g)} + 2e^-$	(3)
	$O_{YSZ}^{2-} \rightarrow [O^{\delta-} - \delta +] + 2e^-$	(4)

The parallel electrical circuit analogy (Achenbach, 1994) is used for the calculation of the total current density distributions of the anode and the cathode:

$$J^C = 3J_1^C, \quad J^A = J_3^A + J_4^A + J_4^A \quad (5)$$

where $J_i^{A/C}$ are the current densities at the Anode/Cathode, respectively and are given by the

Butler–Volmer equation (Tseronis et al., 2012).

2.3 The Catalytic Surface Dynamics

Due to potential application in the pellet and after electrochemical reaction (4) takes place, BSS is formed at the TPB of the anode and migrates over the catalytic film. While diffusing over the catalyst, it can either react with co-adsorbed CO forming CO_2 (the desorption of which is considered as immediate), or desorbs to the gaseous phase as O_2 . These reactions are augmented by the main heterogeneous CO oxidation mechanism (Kaul et al., 1987). The micro-processes that describe the combined, closed-circuit, Electro-Catalytic CO oxidation mechanism are illustrated in Table 2.

Table 2: The scheme of Electro-Catalytic micro-processes.

<i>Open-circuit CO oxidation micro-processes</i>	
$O_{2(g)} + 2* \xrightleftharpoons[k_{-6}]{k_6} 2O*$	(6)
$CO_{(g)} + * \xrightleftharpoons[k_{-7}]{k_7} CO*$	(7)
$O* + CO* \xrightarrow{k_8} CO_{2(g)} + 2*$	(8)
<i>Closed-circuit additional micro-processes</i>	
$[O^{\delta-} - \delta +]* + CO* \xrightarrow{k_9} CO_{2(g)} + 2*$	(9)
$2[O^{\delta-} - \delta +]* \xrightarrow{k_{10}} O_{2(g)} + 2*$	(10)
$X* + * \xrightarrow{k_{diff}} * + X* \quad , \quad X = CO, BSS$	(11)

The transition probabilities of the micro-processes (6-8) can be found in the literature (Reese et al., 2001; Hari and Theodoropoulos, 2009) while the closed-circuit additional ones are expressed as:

$$\begin{aligned} \hat{\Gamma}_9 &= k_9 \cdot (P_{CO*} \cdot P_{BSS*/CO*} + P_{BSS*} \cdot P_{CO*/BSS*}) \\ \hat{\Gamma}_{10} &= k_{10} \cdot (P_{BSS*} \cdot P_{BSS*/BSS*}) \\ \hat{\Gamma}_{X,diff} &= k_{X,diff} \cdot (P_{X*} \cdot P_{*/X*} + P_* \cdot P_{X*/*}) \end{aligned} \quad (12)$$

where P_{X*} and $P_{X*/Y*}$ are one and two-site conditional probabilities respectively.

3 ELECTROCHEMICALLY PROMOTED CO OXIDATION

The proposed multi-scale framework integrates a 3D

macroscopic model which employs the Finite Element Method (FEM) for the simulation of charge conservation in the system and a 2D microscopic one which employs the kinetic Monte Carlo (kMC) method in combination with Gap-Tooth interpolation techniques for the simulation of the reaction-diffusion micro-processes taking place on the catalytic surface. The numbering of the boundaries (B) and edges (E) of the 3D computational domain is presented in Fig. 3.

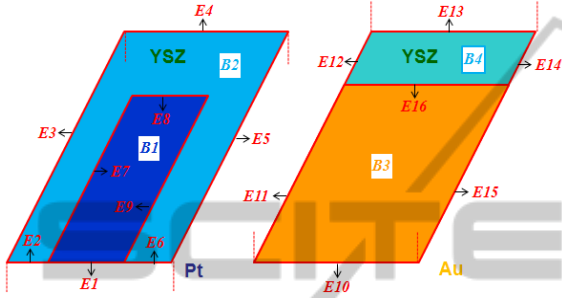


Figure 3: Numbering of Boundaries and Edges.

There are in total 8 boundaries and 20 edges where 4 of which (E7-9 & E16) represent TPBs. Boundaries B1 and B3 represent the Pt and Au electrodes respectively.

3.1 Macroscopic Modelling

3.1.1 Charge Transfer

Under potential application in the pellet, electrochemical reactions take place at the TPBs and ionic as well as electronic charge transport in the electrolyte and the electrodes, respectively. Considering a no charge source, the charge conservation equation of a phase j , takes the following form:

$$\frac{d\rho_j}{dt} = -\nabla \cdot (-\sigma_j \nabla \Phi_j) \quad , \quad j = el, io \quad (13)$$

where ρ_j , σ_j and Φ_j are the charge density, the charge conductivity and the local electrostatic potential respectively, of the phase j . Also, el (B1&B3) and io

(YSZ) denote electronic and ionic current, respectively.

3.1.2 Boundary Conditions

Under closed-circuit conditions, the electronic potential is fixed to the value of the operating potential Φ_{pellet} ($\Phi_{el}^C = \Phi_{\text{pellet}}$) at E10 and electronic charge is transferred through the cathodic electrode (B3). At E16, the electrochemical reduction of O_2 takes place (Rxn 1) and resulting in the conversion of current from electronic to ionic (Eq. 14).

$$-\mathbf{n} \cdot (-\sigma_{el}^C \nabla \Phi_{el}^C) = J^C, \quad -\mathbf{n} \cdot (-\sigma_{io} \nabla \Phi_{io}) = -J^C \quad (14)$$

Ionic charge is then transferred throughout YSZ. Consequently, ionic current is converted to electronic at E7-9 (Eq. 15), due to the electrochemical reactions (Rxn 2-4).

$$-\mathbf{n} \cdot (-\sigma_{io} \nabla \Phi_{io}) = J^A, \quad -\mathbf{n} \cdot (-\sigma_{el}^A \nabla \Phi_{el}^A) = -J^A \quad (15)$$

Electronic charge is transferred through the anodic electrode (B1). At E4 the electronic potential is fixed to zero ($\Phi_{el}^A = 0$). Insulation is imposed for all the remaining boundaries and edges for both electronic and ionic phases.

3.2 Microscopic Modelling

Species reaction and diffusion on the catalytic surface are simulated a spatial version of kMC (Reese et al., 2001). Furthermore, to enable our multi-scale simulator to handle relatively large surfaces (on the order of μm or even mm) we have employed the *gap-tooth* method (Gear et al., 2002, 2003). Here, we represent the catalytic lattice consisting of 1100 by 100 sites with 5 smaller lattices (teeth) of 100 by 100 sites. The distance (gap) between the teeth is constant and equal to 150 sites ($d=150$, $D=250$). The schematic representation of the gap-tooth geometry is depicted in Fig. 4.

The lateral interactions between the teeth, i.e. diffusion of species amongst the lattices, are described by exchange fluxes of particles (as in Fig. 4), here noted as $O_{s,i,k}$, $I_{s,i,k}$ (Outgoing_(side, tooth, particle)).

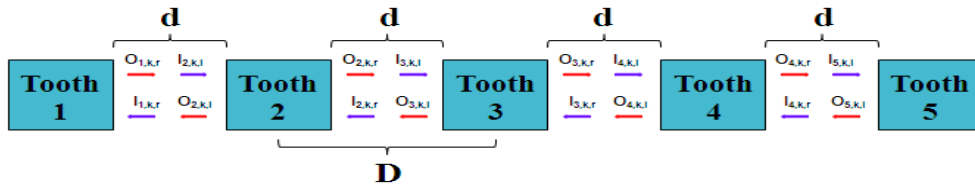


Figure 4: Schematic of the gap-tooth geometry.

Ingoing_(side,tooth,particle)). The expressions that describe the exchange fluxes between two teeth are based on linear interpolation and can be written as:

$$\begin{aligned} I_{R,i,k} &= \alpha_x \cdot O_{L,i+1,k} + (1 - \alpha_x) \cdot O_{L,i,k} \\ I_{L,i,k} &= \alpha_x \cdot O_{R,i-1,k} + (1 - \alpha_x) \cdot O_{R,i,k} \end{aligned} \quad (16)$$

where α_x is an interpolation coefficient which depends on the gap-tooth geometry and is expressed as $\alpha_x = d/D = 0.4$, where d is the length of each tooth and D is the distance between the centre of two teeth (Fig. 4). These exchange fluxes are updated at 1/10 of the reporting horizon ($T = 1e-5$ s) of the kMC simulator.

3.3 The Multiscale Framework

The multiscale framework is illustrated in Fig. 5. Initial conditions such as temperature, T , partial pressures in the gas phase mixture, P_i , and applied potential, Φ_{pellets} , are fed into the microscopic simulator, which employs lattice kMC combined with the Gap-Tooth method to model reaction and diffusion phenomena on the catalyst. At the end of a time reporting horizon (T) the partial pressures are updated due to the Non-Faradaic electro-catalytic rates:

$$\begin{aligned} P_{CO_2}^A &= \frac{RT}{F_d} \left\{ \int_0^{w_p} \int_0^{L_p} \left[(\hat{\Gamma}_7 + \hat{\Gamma}_8) N_s + \frac{J_2^A}{2F} \right] dx dz \right\} \\ P_{CO}^A &= P_{CO}^m - \frac{RT}{F_d} \left\{ \int_0^{w_p} \int_0^{L_p} \left[(\hat{\Gamma}_6 - \hat{\Gamma}_{-6}) N_s + \frac{J_2^A}{2F} \right] dx dz \right\} \\ P_{O_2}^{A/C} &= P_{O_2}^m - \frac{RT}{F_d} \left\{ \int_0^{w_p} \int_0^{L_p} \left[(\hat{\Gamma}_5 - \hat{\Gamma}_{-5} - \hat{\Gamma}_9) N_s - \frac{J_3^A}{4F} \right] dx dz \right. \\ &\quad \left. + \int_0^{w_{tu}} \int_0^{L_{tu}} \frac{J^C}{4F} dx dz \right\} \end{aligned} \quad (17)$$

where P_i is the partial pressure of species i , F_d is the volumetric flowrate of gas mixture in the inlet/outlet of the reactor, N_s is the concentration of the active surface sites on the catalytic surface, W and L are the width and the length of the each electrode respectively, $J_i/n_e F$ is the Faradaic rate resulting by the electrochemical reactions i . The expressions in the curly brackets represent the consumption and production rates of each species.

The computed partial pressures are subsequently fed into the macroscopic simulator, constructed in COMSOL Multiphysics, which employs the FEM for the simultaneous solution of the set of electronic and ionic charge balances. At the end of the same time reporting horizon, T , partial pressures are updated again and fed back to the microscopic simulator also providing a flux for BSS:

$$E7-9: -\mathbf{n} \cdot (-D_{BSS} \nabla \theta_{BSS}) = J_4^A A_s (2FN_s l_{TPB})^{-1} \quad (18)$$

where J_4^A is the anodic current density due to BSS formation at the anodic TPB, A_s is the Pt surface area, l_{TPB} is the TPB length, N_s is the molar concentration of surface sites. These macroscopic inward fluxes are translated as BSS molecules per unit time so as to be used in the microscopic model.

This process is repeated until the desired time is reached.

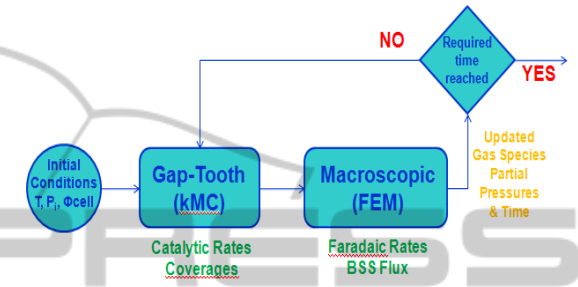


Figure 5: Schematic of the multi-scale framework.

4 COMPUTATIONAL RESULTS

Before applying the gap-tooth method in the multi-scale framework, we have undertaken a validation of our gap-tooth simulator against a single (large) lattice using only the diffusion micro-process for only one species and for a very high - 10^6 - diffusion probability.

In Fig. 6a-e a comparison between the coverage of the diffusing species computed by the single lattice simulation (1100x100 sites) and that computed by the Gap-Tooth simulation (as presented in Fig. 4), utilizing an influx of 100 species per 10^{-4} sec at the left side boundary of tooth 1 and at the left side boundary of the single lattice, respectively, is depicted. As we can see the Gap-Tooth simulator can accurately capture both short and long term dynamics of the diffusing species. This allows us to use the Gap-Tooth simulator in our main modelling study for simulation time up to 10^{-2} sec with confidence. We should note that the for the validation presented here a high - 10^6 - diffusion probability has been used on purpose to enables us to detect the features of the system for the simulated times.

In our multi-scale framework, the macro- and micro-scopic models are linked through a Matlab interface and are simulated iteratively. The gas phase of the system (Fig. 2) was assumed to be well mixed at 1atm, 623.15K, $P_{CO} = 500$ Pa, $P_{O_2} = 5$ kPa and

an applied potential of 500mV. The chosen reaction coefficients are tabulated in Table 3, while the diffusion probabilities of CO and of BSS were chosen as 1, 10^3 and 10^6 in order to illustrate the diffusional effects on the lateral (lattice-to-lattice) interactions between the kMC teeth.

Table 3: The model parameters.

$\gamma_2 = 6.4 \cdot 10^8 \text{ A/m}^2$	$E_{.6} = 222265 \text{ J/mol}$
$\gamma_3 = 5.2 \cdot 10^7 \text{ A/m}^2$	$E_{.7} = 109954 \text{ J/mol}$
$\gamma_4 = 5.9 \cdot 10^5 \text{ A/m}^2$	$E_8 = 39777 \text{ J/mol}$
$S_{CO} = 0.3623$	$k_9 = 1.0310^{-2} \text{ s}^{-1}$
$S_{O_2} = 0.0106$	$k_{10} = 8.810^{-3} \text{ s}^{-1}$

In Fig. 7a-e a comparison between the coverage of CO (main diffusing adsorbate) computed by the multi-scale simulation of the large (1100x100 sites) lattice and that computed by the CFD-kMC-gap-tooth scheme is depicted. As we can see the latter can accurately capture the long and short term dynamics of the main diffusing species (CO) for the whole time range, at a fraction of the computational cost (approximately 16% of the CPU time used by the full-scale simulator) even for the very high - 10^6 - diffusion probability.

We have also investigated the effect of the lattice-to-lattice interactions on the selected system and operating conditions. Thus, we have performed a gap-tooth simulation not considering any lateral interactions (only CO diffusion within each lattice was allowed).

A comparison between the CO average coverage profiles in the single (large) lattice (red lines) and in teeth 1-5 with (green diamonds) and without (blue lines) lattice-to-lattice interactions is presented in Fig. 8. The value of 10^6 was selected as a diffusion probability because for this value, diffusion events represent 60% of the total micro-processes on the lattice, hence we can more clearly see the effect of diffusion on the system. As we can observe in Fig. 7 the single lattice is very well represented using the gap-tooth simulator, with lateral interactions, while some differences exist for the case of no lateral interactions as expected. Nevertheless, due to the dominant presence of catalytic reactions (6-8) these differences are small.

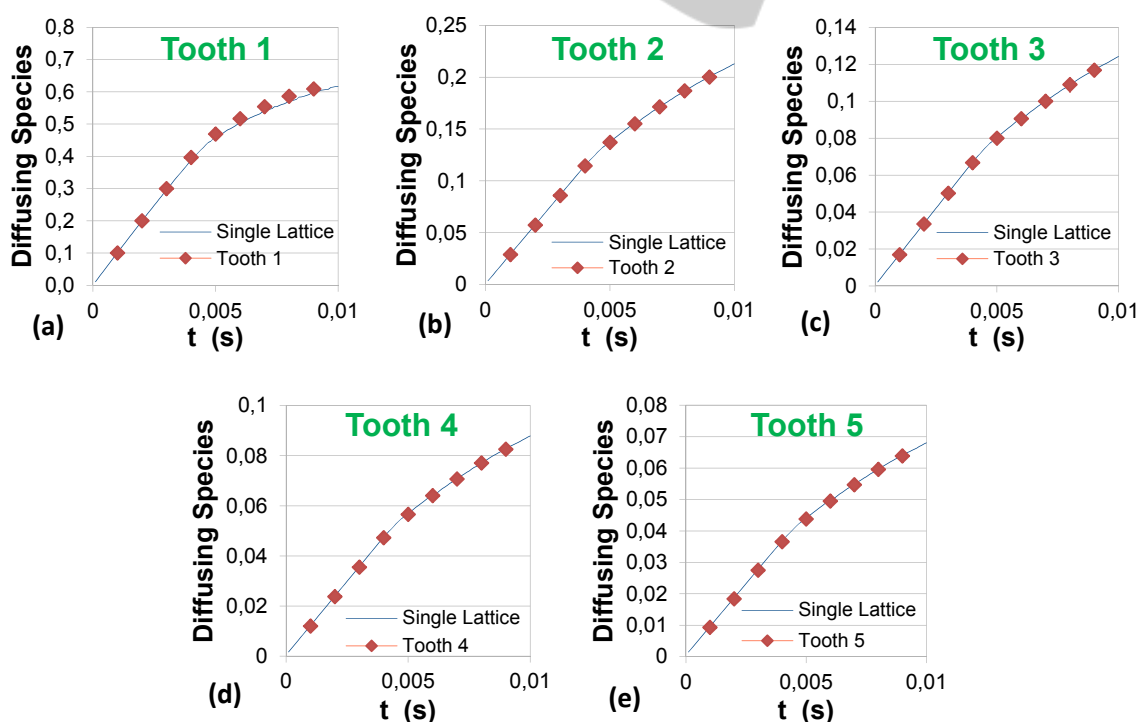


Figure 6: Diffusing species average coverage profiles comparison, between a Single Lattice and, (a) Tooth 1, (b) Tooth 2, (c) Tooth 3, (d) Tooth 4, (d) Tooth 4, (e) Tooth 5, for a 10^6 chosen diffusion probability.

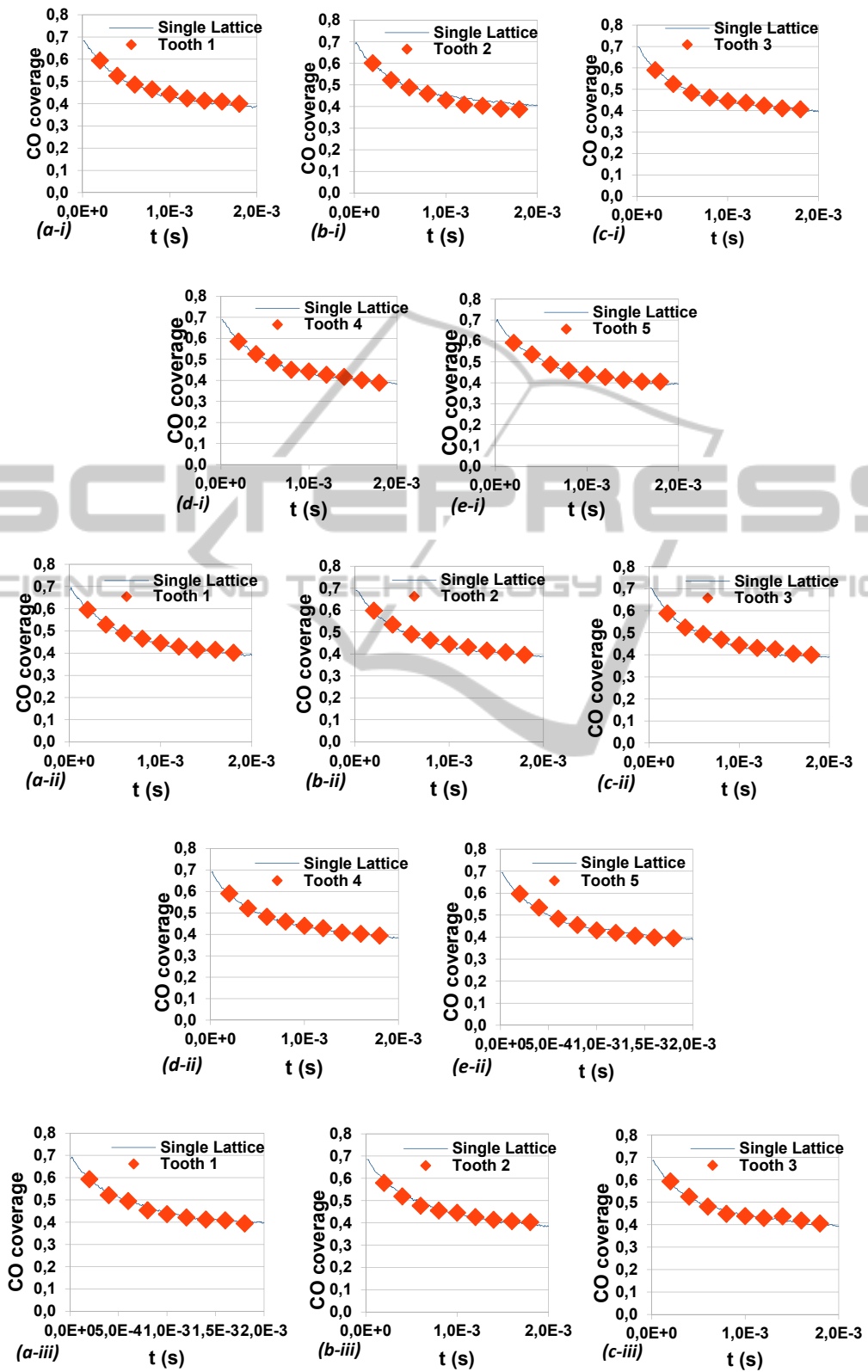


Figure 7: CO average coverage profiles comparison, between a Single Lattice and (a) Tooth 1, (b) Tooth 2, (c) Tooth 3, (d) Tooth 4, (e) Tooth 5. The (i), (ii) and (iii) represent results utilizing 1, 10^3 and 10^6 diffusion probabilities respectively.

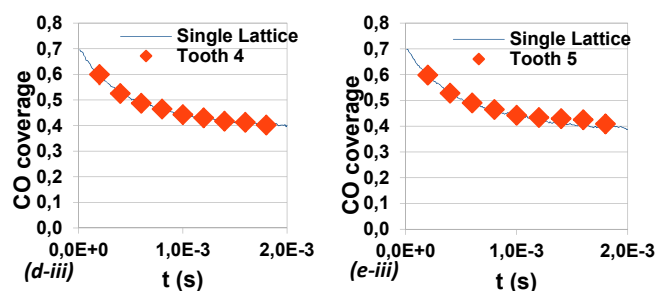


Figure 7: CO average coverage profiles comparison, between a Single Lattice and (a) Tooth 1, (b) Tooth 2, (c) Tooth 3, (d) Tooth 4, (e) Tooth 5. The (i), (ii) and (iii) represent results utilizing 1, 10^3 and 10^6 diffusion probabilities respectively. (Cont.)

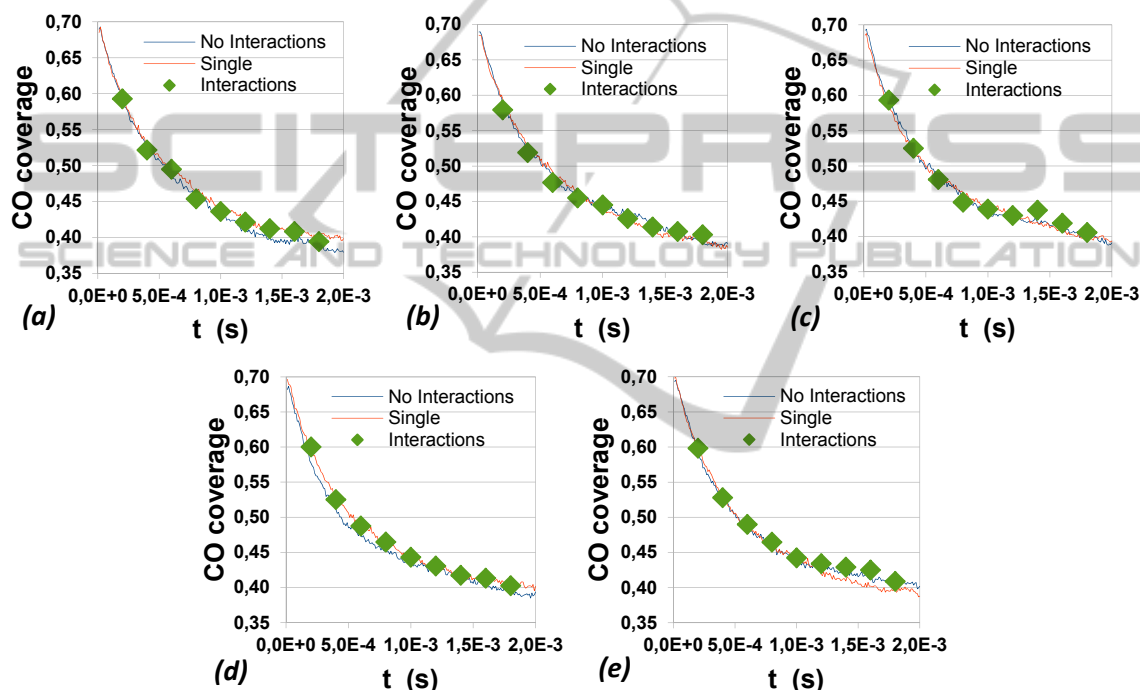


Figure 8: CO average coverage profiles comparison, between a Single Lattice and, (a) Tooth 1, (b) Tooth 2, (c) Tooth 3, (d) Tooth 4, (e) Tooth 5, with and without lattice-to-lattice internal interactions, for a 10^6 chosen diffusion probability.

5 CONCLUSIONS

A multiscale framework for an Electrochemically Promoted system has been presented. It integrates a macroscopic model for the simulation of charge conservation in the system and a microscopic one using an in house developed lattice kMC simulator and the Gap-Tooth method for the simulation of the catalytic surface dynamics. This simulator can accurately capture the surface dynamics with computational efficiency enabling us to simulate larger realistic systems. This framework in conjunction with high-fidelity experiments

(currently underway) will lead to the computation of reliable system parameters and towards optimal and robust system design scale-up and control or electrochemically-promoted systems.

ACKNOWLEDGEMENTS

The financial support of EPSRC (grant EP/G022933/1) is gratefully acknowledged.

REFERENCES

- Achenbach, E., 1994. *Three-dimensional and time-dependent simulation of a planar solid oxide fuel cell stack*. Journal of Power Sources, 49, (1-3): 333-348.
- Armaou, A., Kevrekidis, I. G., Theodoropoulos, C., 2005. *Equation-free gaptooth-based controller design for distributed complex/multiscale processes*. Computers and Chemical Engineering, 29, (4): 731-740.
- Fragkopoulou, I. S., Bonis, I., Theodoropoulos, C., 2012. *Multiscale modelling of spillover processes in heterogeneous catalytic systems*. Computer Aided Process Engineering, 30, 1013-1017.
- Gear, C. W., Kevrekidis, I. G., Theodoropoulos, C., 2002. *'Coarse' integration/bifurcation analysis via microscopic simulators: Micro-Galerkin methods*. Computers and Chemical Engineering, 26, (7-8): 941-963.
- Gear, C. W., Li, J., Kevrekidis, I. G., 2003. *The gap-tooth method in particle simulations*. Physics Letters A, 316, 190-195.
- Hari, B., Theodoropoulos, C., 2009. *Integrated multi-scale models for simulation and design of microreactor systems*. Chemical Engineering Transactions: 9th International Conference on Chemical and Process Engineering, 17, 1269-1274.
- Kaul, D. J., Sant, R., Wicke, E. E., 1987. *Integrated kinetic modeling and transient FTIR studies of CO oxidation on Pt/SiO₂*. Chemical Engineering Science, 42, (6): 1399-1411.
- Poulidi, D., Rivas, M. E., Metcalfe, I. S., 2011. *Controlled spillover in a single catalyst pellet: Rate modification, mechanism and relationship with electrochemical promotion*. Journal of Catalysis, 281, (1): 188-197.
- Reese, J. S., Raimondeau, S., Vlachos, D. G., 2001. *Monte Carlo Algorithms for Complex Surface Reaction Mechanisms: Efficiency and Accuracy*. Journal of Computational Physics, 173, (1): 302-321.
- Stoukides, M., Vayenas, C. G., 1981. *The effect of electrochemical oxygen pumping on the rate and selectivity of ethylene oxidation on polycrystalline silver*. Journal of Catalysis, 70, (1): 137-146.
- Tseronis, K., Bonis, I., Kookos, I. K., Theodoropoulos, C., 2012. *Parametric and transient analysis of non-isothermal, planar solid oxide fuel cells*. International Journal of Hydrogen Energy, 37, (1): 530-547.
- Yentekakis, I.V., Moggridge, G., Vayenas, C.G., Lambert, R.M., 1994. *In Situ controlled promotion of catalyst surfaces via NEMCA: The effect of Na on Pt-catalyzed CO oxidation*. Journal of Catalysis, 146, (1): 292-305.